Spectrochimica Acta Part A: Molecular and Biomolecular Spectroscopy 222 (2019) 117218

Contents lists available at ScienceDirect

Spectrochimica Acta Part A: Molecular and Biomolecular Spectroscopy

journal homepage: www.elsevier.com/locate/saa

Colorimetric immunosensor for determination of prostate specific antigen using surface plasmon resonance band of colloidal triangular shape gold nanoparticles

Pari Karami [a], Hosein Khoshsafar [a], Mohammad Johari-Ahar [b,c], Fabiana Arduini [d], Abbas Afkhami [e], Hasan Bagheri [f,*]

[a] Research and Development Department, Farin Behbood Tashkhis LTD, Tehran, Iran
[b] Department of Medicinal Chemistry, School of Pharmacy, Ardabil University of Medical Sciences, Ardabil, Iran
[c] Biosensor Research Center (BRC), Ardabil University of Medical Sciences, Ardabil, Iran
[d] Department of Chemical Science and Technologies, University of Rome Tor Vergata, Via della Ricerca Scientifica, 00133 Rome, Italy
[e] Faculty of Chemistry, Bu-Ali Sina University, Hamedan, Iran
[f] Chemical Injuries Research Center, Systems Biology and Poisonings Institute, Baqiyatallah University of Medical Sciences, Tehran, Iran

ARTICLE INFO

Article history:
Received 19 March 2019
Received in revised form 12 May 2019
Accepted 27 May 2019
Available online 29 May 2019

Keywords:
Colorimetric immunosensor
Sandwich assay
Surface plasmon resonance
Total prostate specific antigen
Magnetic nanoparticles

ABSTRACT

In this work, we demonstrated the development of a colorimetric immunosensor using surface plasmon resonance band of gold nanoparticles for the detection of prostate specific antigen (PSA). To develop this biosensing tool, triangular gold nanoparticles (AuNPs) were synthesized using Tween-20 as a nonionic surfactant and then, conjugated with PSA capture antibody (Ab_1-AuNPs). When exposed to Ab_1-AuNPs, PSA antigens were found to be successfully captured by nanosystem (PSA)-Ab_1-AuNPs. Next, (PSA)-Ab_1-AuNPs were incubated with second PSA antibody (2)-decorated magnetite (Fe_3O_4-Ab_2) and separated by an external magnetic force to leave Ab_1-AuNPs in the supernatant solution to be directly analyzed using UV–Vis spectroscopy. It was found that the absorption intensity was directly proportional to the PSA concentration. As a result, the linear range for PSA detection was found to be 0.01–20 ng mL^{-1} with a detection limit of 0.009 ng mL^{-1}. Because of significant stability of the prepared Ab_1-AuNPs and excellent selectivity to the PSA antigen, this simple and sensitive sensing system is proposed to be potentially effective in the fast and real-time analysis of clinical samples from prostate cancer patients. We believe that the simple platform of this immunosensor to be useful in the development of future point-of-care sensing tools, working on the quantification of biomarkers in a drop of blood.

1. Introduction

Prostate specific antigen (PSA) is a glycoprotein that generally exists in healthy adult males below 4 ng mL^{-1}, but clinically, abnormal levels of PSA is an important serum biomarker for early and differential diagnosis of benign prostatic hyperplasia (BPH) and prostate cancer and evaluation of patient's response to chemotherapy [1,2]. In this way, it is really important to establish new sensing methods to approach simple, rapid and accurate detection of such biomarker for early-stage diagnosis of prostate cancer to avoid unpredictable metastasis.

Till now, a variety of assays such as chromatography [3], mass spectroscopy [4], fluorescence spectroscopy [5], nuclear magnetic resonance spectroscopy [6], white light reflectance spectroscopy [7], capillary electrophoresis [8], chemiluminescence [9], enzyme-linked immunosorbent assays (ELISA) [10], electrochemiluminescence [11,12], radioimmunoassay [13], time-resolved immunofluorometric assay [14], surface plasmon fluorescence immunoassay [15], bioluminescent immunoassay [16], electrochemical [17], surface-enhanced Raman scattering [18], and microcantilever method [19] have been developed for the determination of PSA. These methods unfortunately encounter with challenges for clinical applications, necessitating skilled personnel working with expensive, time-consuming and complex technology [20–22].

In attempt to removing such limitations, sandwich-type colorimetric immunoassays based on lateral surface plasmon resonance as a noninvasive strategy have represented capacity of simplicity, low-cost translation, and tailoring to point-of-care applications.

With introduction of nanomedicine, a convergence of nanoscience and medicine, nanomaterials have attracted great attention in all fields

* Corresponding author.
E-mail address: h.bagheri@bmsu.ac.ir (H. Bagheri).

https://doi.org/10.1016/j.saa.2019.117218
1386-1425/

of science [23–28]. Of various nanoparticles exploited in the era of bioanalytical sciences, gold nanoparticles with different sizes and shapes have been successfully used as a signaling probe for sensitive analysis of cancer biomarkers [29,30]. Due to having unique and tunable surface plasmon resonance (SPR) properties, gold nanoparticles (AuNPs) have been the subject of intensive research on UV–Vis extinction bands. When the frequency of an incident photon with the conduction electrons of AuNPs is in proper resonance, SPR as wavelength-selective absorption with extremely large molar extinction coefficients can be induced [31].

Due to having a narrow plasmon peak, stability in the complex system of biological samples, and greater molar extinction coefficient, non-spherical gold nanoparticles especially triangular AuNPs are prone to improve sensitivity of detection and to lower the limit of detection. Triangular AuNPs significantly exhibit excellent stability at high salt concentrations (0.1 mol L^{-1}), and are laborious to separate [31]. To reach efficient separation, application of magnetic nanoparticles in connection with gold nanoparticles leads to approaching lower detection limits and fast responsive biosensors [32]. In the field of bio-separation, Magnetic nanoparticles are defined as core nanomaterials and magnetite (Fe_3O_4) nanoparticles are generally used to magnetically isolate proteins, DNA, viruses and even whole mammalian cells [33].

In this work, we demonstrate the development of a colorimetric sandwich-type immunosensor for detection of PSA using lateral surface plasmon resonance of triangular AuNPs and magnetic force separation of Fe_3O_4 NPs decorated with PSA-specific antibodies (Ab_1-AuNPs and Fe_3O_4-Ab_2).

2. Materials and methods

2.1. Chemicals

Tween-20, NaOH, HCl, K_2HPO_4, and KH_2PO_4 were purchased from Merck (Darmstadt, Germany). 3-(Trimethoxysilyl)-propylamine (APTS), acetic acid, hydrogen tetrachloroaurate ($HAuCl_4.3H_2O$, 99.5%), magnetite (Fe_3O_4) and hexane were obtained from Sigma-Aldrich company. (St. Louis, Missouri, United States). Monoclonal anti-PSA antibodies (Ab_1 (1H12, epitope 4) and Ab_2 (5A6, epitope 6)) were obtained from HyTest (Turku, Finland). PSA ELISA kit was purchased from (R&D Systems, Minneapolis, MN, USA). All solutions were prepared with deionized water with a specific resistance 18.2 MΩ × cm (million ohms) at 25 °C. (Merck Millipore, Darmstadt, Germany). All of the glassware was cleaned by aqua regia (HCl: HNO_3 in a 3: 1 ratio by volume) and rinsed with water prior to the experiments.

2.2. Apparatus

UV–Vis spectroscopy was performed on a Perkin–Elmer Lambda 25 spectrophotometer with the use of semi-micro spectrophotometric cuvettes. Transmission electron microscopy (TEM) images were recorded using a Philips CM10 TEM (USA) at an accelerating voltage of 80 kV. The size distributions of the nanoparticles were obtained using Nanotrac Wave™ (Microtrac, San Diego, CA, USA). The size of nanoparticles was calculated by fitting the data to a polydispersed model using the Dynamics software version 5.26 (Microtrac, San Diego, CA, USA).

2.3. Preparation of Ab_1-AuNPs

The AuNPs were prepared based on our previously reported method [31]. Briefly, 4 mL of Tween-20 solution 20% (v/v) in PBS (pH = 7.0) was added to 1 mL of $HAuCl_4$ (10 mmol L^{-1}). Carboxylic functional groups of tween-20 were activated using a solution containing EDC (20 mg mL^{-1}) and NHS (10 mg mL^{-1}) in borate buffer (pH = 9) under shaking (60 rpm) at room temperature and dark for 30 min.

To covalently attach AuNPs with Ab_1, the activated nanoparticles were incubated with Ab_1 (50 μg mL^{-1}) solution at 8 °C and dark under shaking (60 rpm) for 24 h. after washing with Tween-20 solution 20% (v/v) to remove unconjugated Ab_1, the antibody-conjugated Au NPs (Ab_1-AuNPs) were centrifuged at 4000 ×*g* for 5 min, and finally the precipitation was finally dispersed and stored in a solution containing 0.1% sodium azide at 4 °C for next applications.

2.4. Preparation of Ab_2-Fe_3O_4

The Fe_3O_4 NPs were prepared by the silanization method [34]. Initially, in a glass container under ambient conditions, 0.5% (v/v) APTS solution was added to a dispersion of Fe_3O_4 solution (0.5 mg mL^{-1}) in hexane containing 0.01% (v/v) acetic acid. The mixture was shaken for 72 h during which the nanoparticles were precipitated. The APTS-modified Fe_3O_4 NPs (APTS-Fe_3O_4) were separated using an external magnet and then washed with hexane three times to remove all unreacted silanes. The product was finally redispersed in deionized (DI) water.

Carboxylic functional groups of APTS-Fe_3O_4 were activated using a solution containing EDC (20 mg mL^{-1}) and NHS (10 mg mL^{-1}) in borate buffer (pH 9) under shaking (60 rpm) at room temperature and dark for 30 min.

To covalently attach APTS-Fe_3O_4 (0.2 mg mL^{-1}) NPs with Ab_2, the activated NPs were incubated with Ab_2 (50 μg mL^{-1}) solution at 8 °C and dark under shaking (60 rpm) for 24 h. The prepared Fe_3O_4-Ab_2 NPs were separated using an external magnet and then washed with DI water three times to remove all unconjugated Ab_2 molecules. The final product was dispersed in PBS buffer (10 mmol L^{-1}) containing 0.1% sodium azide and stored at 4 °C for next applications.

2.5. Determination of PSA

In order to analyze PSA, 1.5 mL of standard solutions (1 mmol L^{-1} PBS, pH = 7.4) containing distinctive content of PSA were incubated with 50 μL of Ab_1-AuNPs (0.1 mg mL^{-1}). The shaker incubator with a rotation speed of 200 rpm at 25 °C for 70 min was used for the completion of antigen-antibody reactions.

Afterward, 50 μL of Fe3O4-Ab_2 suspension was added and incubated with a rotation speed of 200 rpm on a shaker at 25 °C for 60 min. After magnetic separation (MS) of the formed immune-complexes (Fe3O4-Ab_2-(PSA)-Ab_1-AuNPs), a portion of the supernatant was directly transferred into semi-micro spectrophotometer cuvettes for measurement of absorption.

The absorptions were recorded at 525 nm as the λ_{max} of Au NPs SPR. Final absorption was calculated by subtracting the absorption of the corresponding blank samples. In order to confirm the reproducibility, each immunoassay had to be completed in triplicate. Scheme 1 illustrates the principle of the immunosensor development.

2.6. Serum sample analysis

The potential basic and clinical applicability of the immunosensor was tested for the determination PSA in blood serum samples obtained from healthy and patient volunteers. The results of the immunosensor were compared with those of ELISA method. The samples were diluted 2-fold by 1 mmol L^{-1} PBS (pH 7.0) before analysis.

3. Results and discussion

3.1. Characteristics of immunosensor

3.1.1. UV-Vis spectroscopy analysis

The engineered immunosensor was first characterized by UV–Vis spectroscopy. As shown in Fig. 1, Panel A, the absorption of bare Fe3O4 (APTS-Fe3O4), Fe3O4-Ab_2 and Fe3O4-Ab_2-(PSA) nanoparticles were the measurement in the range of 200–900 nm. After immobilization of Ab_2 on Fe3O4, an obvious absorption peak appeared at 300 nm

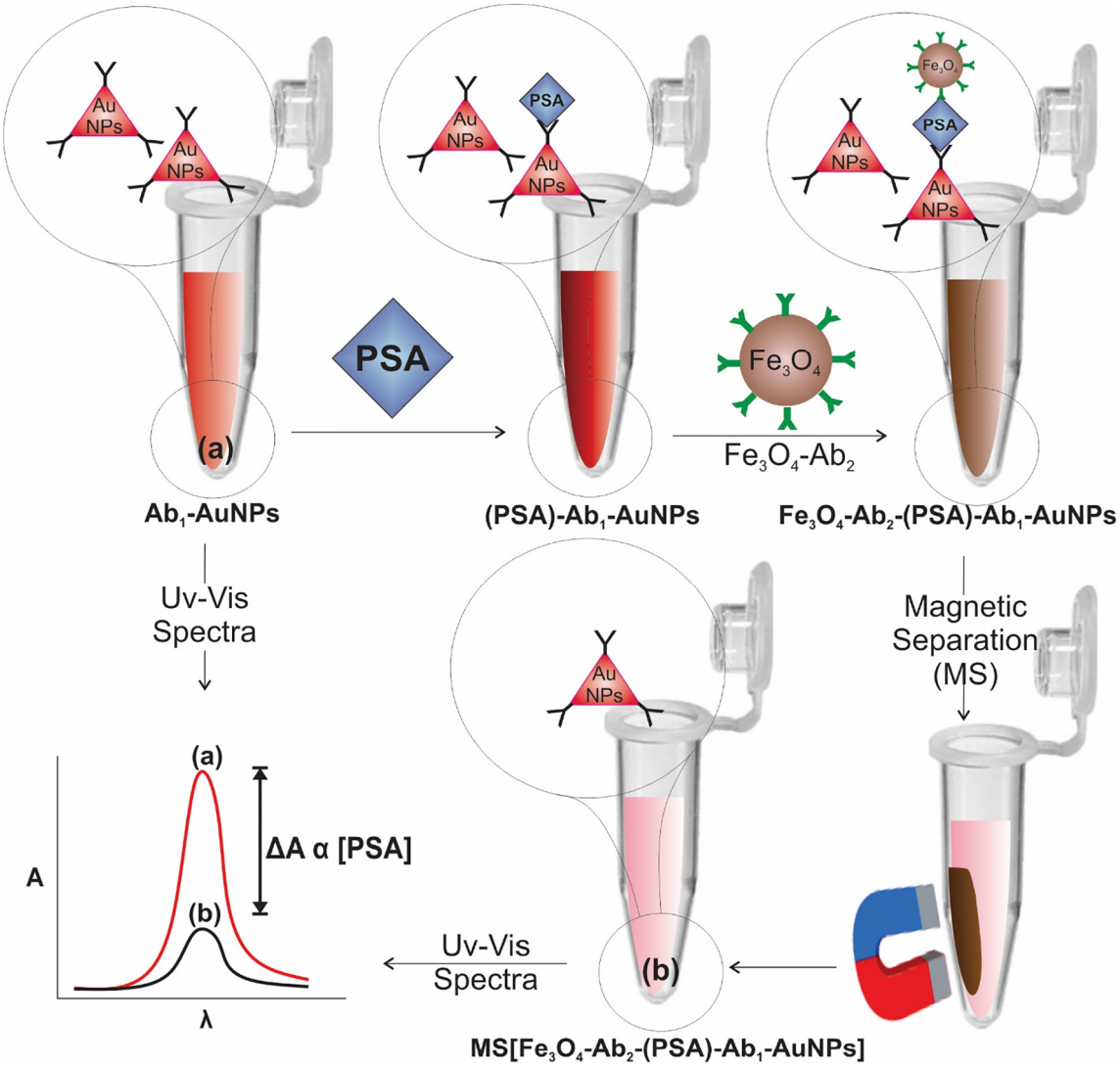

Scheme 1. The performance of the immunosensor.

(curve b), which can be an indicator of Ab_2 immobilization on the surface of Fe3O4 NPs. After the interaction of PSA and Fe3O4-Ab_2 (curve c), the slight bathochromic shift in plasmon band position confirms the formation of immuno-complex.

As shown in Fig. 1, Panel B, the bare AuNPs exhibit an absorption peak at 515 nm, ascribing to SPR pf AU NPs (curve j). After being coated with antibodies (Ab_1-AuNPs) (curve k), an obvious absorption peak appeared at 300 nm, indicating the successful immobilization of Ab_1 on the surface of AuNPs and red-shifting of SPR peak from 515 to 525 nm due to the increase in the hydrodynamic diameter of AuNPs. Moreover, the results clearly indicated immune-complexation of PSA and Ab_1-AuNPs (Fig. 1, Panel C, curve e) resulted in an obvious absorption peak at 620 nm, which can be due to the aggregation of Ab_1-AuNPs. After interaction of Fe3O4-Ab_2 and (PSA)-Ab_1-AuNPs, the SPR peak shifted from 620 nm to 725 nm, indicating to the significant increase in the diameter of the formed nano-complex (Ab_1-AuNPs -Fe3O4-Ab_2) (Fig. 1, Panel C, curve f). When magnetic separation was applied on Fe3O4-Ab_2-(PSA)-Ab_1-AuNPs, the UV–Vis absorption of Ab_1-AuNPs decreased significantly (Fig. 1, Panel C, curve g) because the formation of complexation between (PSA)-Ab_1-AuNPs and Fe3O4-Ab_2 led to the dropping of Ab_1-AuNPs concentration in the supernatant. Fig. 1, Panel C, curve h indicates that the absorption peak of Ab_1-AuNPs is not affected by Fe3O4-Ab_2NPs.

3.1.2. TEM and DLS analysis

The size and shape of gold nanoparticles strongly influence their chemical and other properties. The triangular shaped nanoparticles show attractive optical properties in comparison to spherical one [35,36]. So, in the present work, triangular-shaped gold nanoparticles were used instead of conventional citrate-capped gold nanoparticles for constructing colorimetric immunoassay. The prepared NPs were characterized by TEM and DLS, as shown in Fig. 1. As expected, the Fe3O4-Ab_2 NPs were spherical with a mean diameter of 34.5 nm (Panels D_I and D_{II}). As shown in Fig. 1, Panels E_I and E_{II}, Ab_1-AuNPs had a truncated triangular shape with an average edge length of 28.4 nm. The TEM and DLS images of the Fe_3O_4-Ab_2 and Ab_1-AuNPs aggregation in the presence of PSA antigen resulted in the mean diameter of 88.2 nm (Fig. 1, Panels F_I and F_{II}), representing that Fe3O4-Ab_2 and Ab_1-AuNPs have the capability of forming a sandwich structure Fe3O4-Ab_2-(PSA)-Ab_1-AuNPs.

3.2. Optimization of the experimental parameters

3.2.1. Interaction of PSA with Ab_1-AuNPs

To find the optimum incubation time for completion of complex formation between PSA and Ab_1-AuNPs, UV–Vis spectra were recorded at different time points. The results, as shown in Fig. 2, Panel A_I, indicated

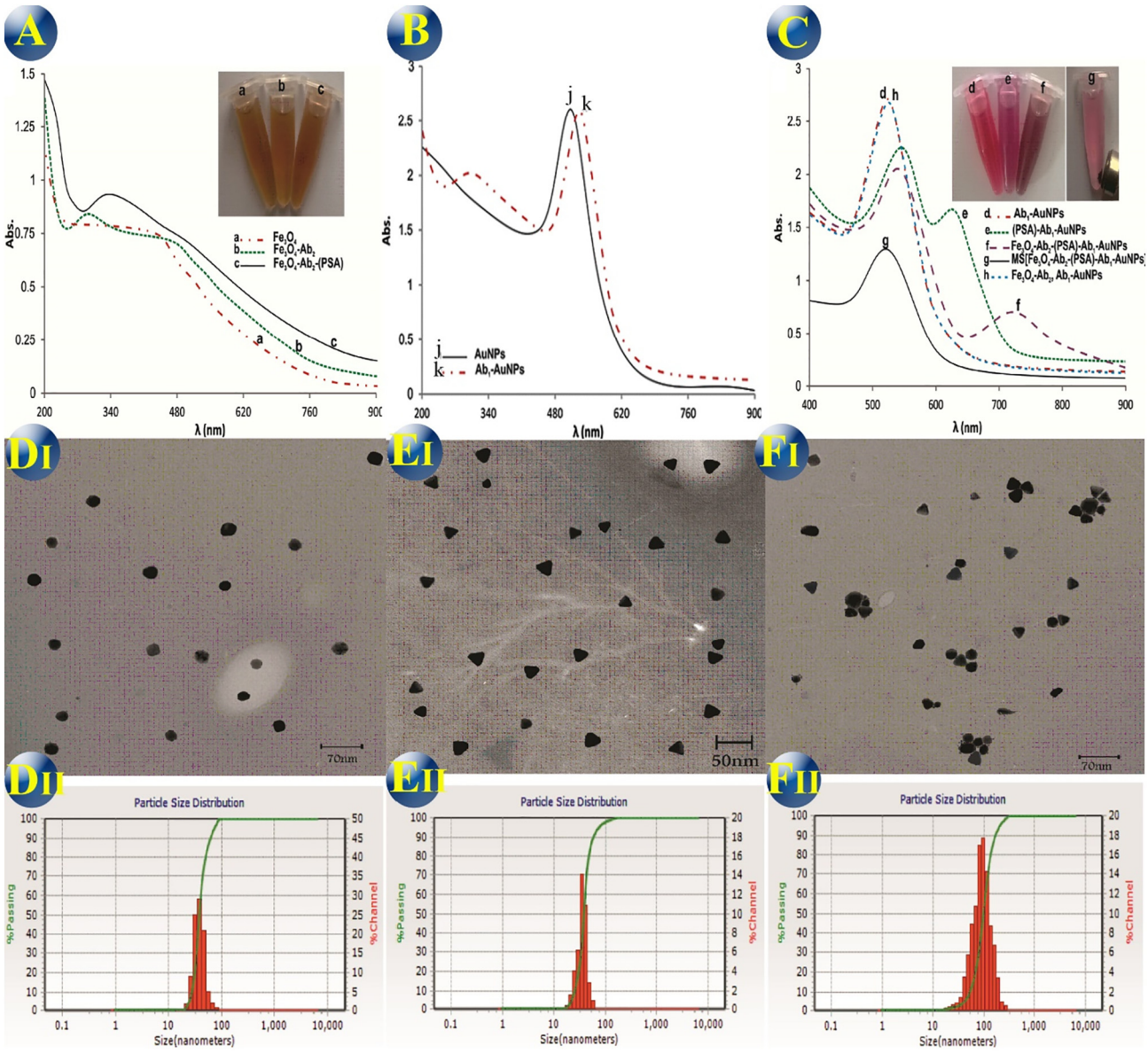

Fig. 1. UV–Vis absorption spectra of (A) APTS- Fe_3O_4 (a), Fe_3O_4-Ab_2 (b) and Fe_3O_4-Ab_2-(PSA) (c), (B) AuNPs (j) and Ab_1-AuNPs (k) and (C) Ab_1-AuNPs (d), (PSA)-Ab_1-AuNPs (e), Fe_3O_4-Ab_2-(PSA)-Ab_1-AuNPs (f), MS [Fe_3O_4-Ab_2-(PSA)-Ab_1-AuNPs] (g) and Ab_1-AuNPs in the presence of Fe_3O_4-Ab_2 (h). (Inset: The visual color change). The TEM image and DLS analysis of Fe_3O_4-Ab2 (DI, DII), Ab_1-AuNPs (EI, EII) and Fe_3O_4-Ab_2-(PSA)-Ab_1-AuNPs (FI, FII) respectively.

with the increase of incubation time (until 70 min), the absorption intensity at 525 nm was declined and intensity at 620 nm increased, showing Ab_1-AuNPs are gradually bound with PSA antigen molecules during 70 min. After 70 min, due to saturation of occupation sites, no significant changes were observed in absorption (Fig. 2, Panel A_{II}). So the optimum incubation time was found to be 70 min.

The formation of the complex between the PSA and Ab_1-AuNPs was studied at four temperatures. As can be seen in Fig. 2, Panel B, with an increase in temperature from 25 °C to 37 °C, absorption at 525 nm was gradually decreased until reaching to its minimum value at 37 °C, suggesting the minimum interaction between PSA and Ab_1-AuNPs. However, the optimum temperature for the interaction of PSA with Ab_1-AuNPs was found to be 25 °C.

3.2.2. Optimization Fe_3O_4-Ab_2 interaction with (PSA)-Ab_1-AuNPs

To find the optimum incubation time for completion of complex formation between Fe_3O_4-Ab_2 with (PSA)-Ab_1-AuNPs, UV–Vis spectra were recorded at different time points. The results, shown in Fig. 2, Panel C_I indicated SPR peak decreased at 525 nm and 620 nm and increased at 725 nm until 60 min. After 60 min, no significant changes were observed in absorption spectra (Fig. 2, Panel C_{II}). So, the optimum incubation time needed for the Fe_3O_4-Ab_2-(PSA)-Ab_1-AuNPs complex formation was found to be 60 min.

The complex formation between the (PSA)-Ab_1-AuNPs and Fe_3O_4-Ab_2 was studied at four different temperatures. As can be seen in Fig. 2, Panel D, with the increase in temperature from 25 °C to 37 °C, absorption at 525 nm was decreased to its minimum value, representing that the good interaction between the (PSA)-Ab_1-AuNPs and Fe_3O_4-Ab_2 occurs. Based on the results, the optimum temperature for maximum interaction of (PSA)-Ab_1-AuNPs with Fe_3O_4-Ab_2 was found to be 25 °C.

3.2.3. Optimization of pH

The performance of the immunosensor and net charges of biomolecules (PSA and antibodies) can be greatly affected by pH adjustment. So the influence of pH on immunosensor performance was investigated in more detail. As nonionic surfactant, Tween-20 was selected as AuNPs stabilizer instead of citrate in this study, steric repulsion between NPs

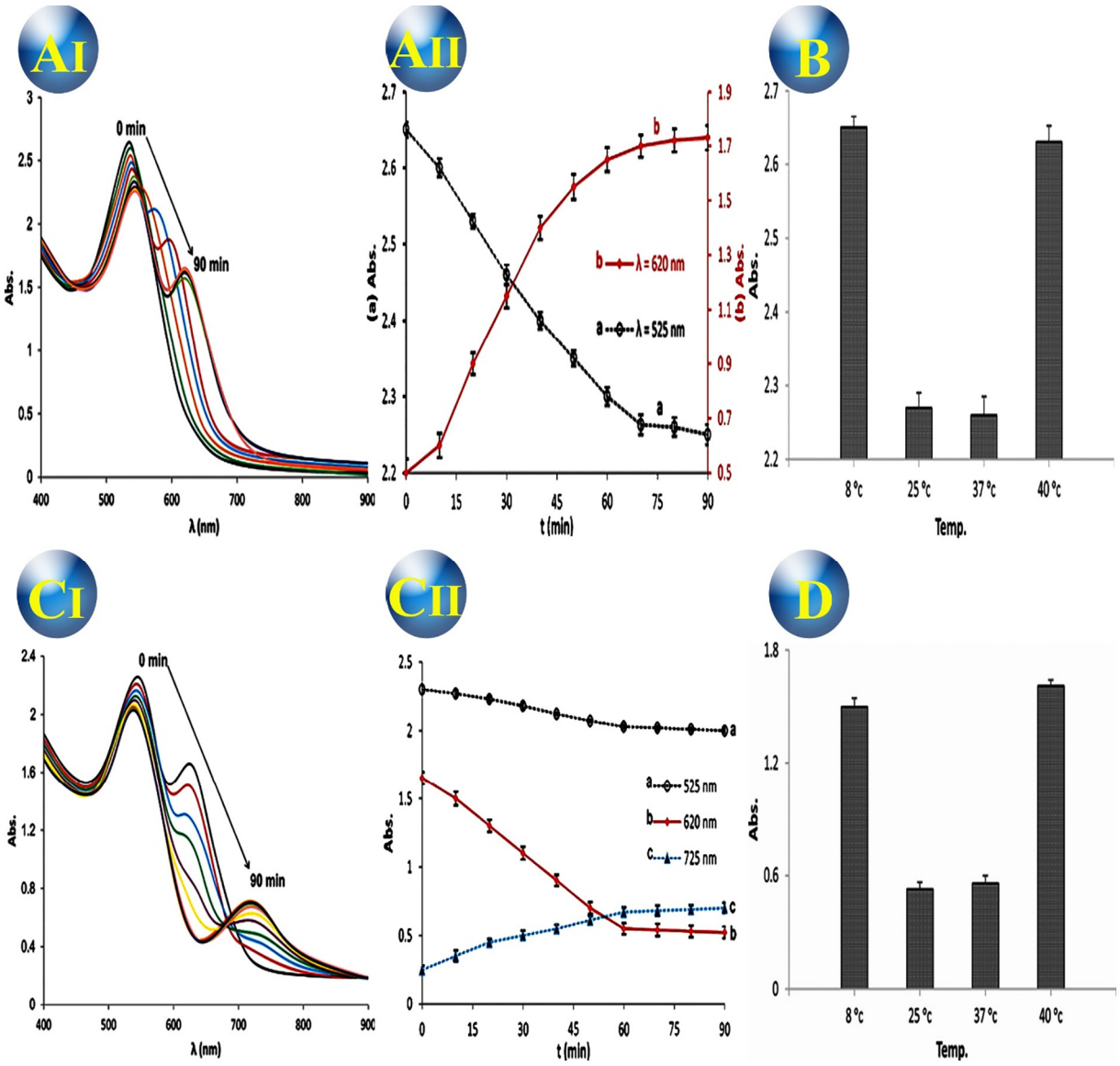

Fig. 2. (AI) UV–Vis absorption spectra of Ab_1-AuNPs in present of 10 ng mL^{-1} PSA at different incubation time (0–90 min). (AII) Variations in the absorption intensity of (PSA)-Ab_1-AuNPs at 525 nm (a) and 620 nm (b) for different incubation time. (B) Variations in the absorption intensity of (PSA)-Ab_1-AuNPs at 525 nm for different incubation temperature. (CI) UV–Vis absorption spectra of (PSA)-Ab_1-AuNPs in present of Fe_3O_4-Ab_2 at different incubation time (0–90 min). (CII) Variations in the absorption intensity of Fe_3O_4-Ab_2-(PSA)-Ab_1-AuNPs at 525 nm (a), 620 nm (b) and 725 nm (c) for different incubation time. (D) Variations in the absorption intensity of Fe_3O_4-Ab_2-(PSA)-Ab_1-AuNPs at 525 nm for different incubation temperature.

resulted from formed layers of tween-20 molecules led to the steric stabilization of the prepared Au NPs and prevent to aggregation of nanoparticles in high ionic strength solutions.

Moreover, the Ab_1-AuNPs, shown in Fig. S1, Panel A (see Supplementary Material), represented remarkable stability over a wide range of pH values (5–9). Fig. S1, Panel B (see Supplementary Material) shows the result of the study on absorption of (PSA)-Ab_1-AuNPs at pH values ranging from 5 to 9. With the increase of pH, the SPR peaks shifted to the red region, and the size of Au NPs increased in contrast to the unreacted NPs. In pH values above 9, (PSA)-Ab_1-AuNPs were completely aggregated (Fig. S1, Panel D, curve a, see Supplementary Material) (Fig. S1, Panel D, curve b, see Supplementary Material). Fig. S1, Panel C (see Supplementary Material) shows the absorption of Ab_1-AuNPs after applying an external magnetic field for separation of Fe_3O_4-Ab_2-(PSA)-Ab_1-AuNPs at the measured pH values. The tighter the interaction of Ab_1-AuNPs with Fe_3O_4-Ab_2 via PSA molecules, the lower the Ab_1-AuNPs in the supernatant and the shorter absorption peak. The greater absorption peaks were observed at pH of 5, 6 and 9, which can be due to the dissociation of Fe_3O_4-Ab_2-(PSA)-Ab_1-AuNPs complex and release of Ab_1-AuNPs. However, based on absorption data, it can be concluded that the most stable complexes are formed at physiological pH.

In addition, the effect of pH on the sensitivity of the immunosensor showed that maximum sensitivity in the performance of the immunosensor is observed in physiological pH values (Fig. S2, see Supplementary Material).

3.3. Analytical features

3.3.1. Determination of PSA

Under the optimized conditions, UV–Vis absorption spectra of the Ab_1-AuNPs, after incubation with Fe_3O_4-Ab_2 in the presence of standard concentrations of PSA were recorded, and the results showed that after applying external magnetic field to isolate Fe_3O_4-Ab_2-(PSA)-Ab_1-AuNPs, the intensity of plasmon absorption peak of Ab_1-AuNPs is inversely proportional to the concentration of PSA (Fig. 3, Panel A). For

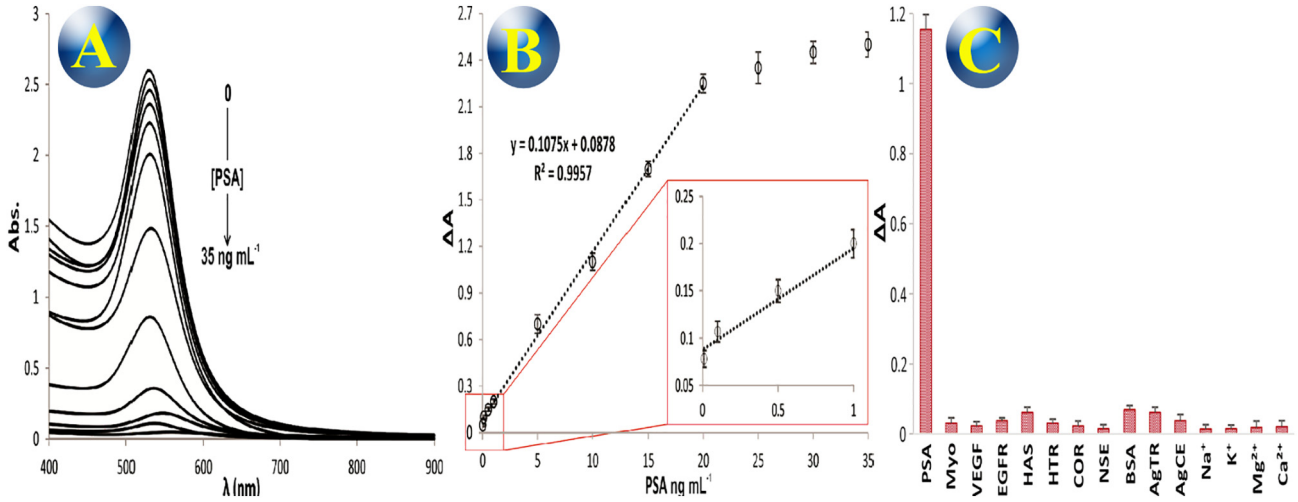

Fig. 3. (A) UV–Vis absorption spectra of the MS [Fe_3O_4-Ab_2-(PSA)-Ab_1-AuNPs] in present of different concentrations of PSA (0, 0.01, 0.1, 0.5, 1, 5, 10, 15, 20, 25, 30 and 35 ng mL^{-1}). (B) Variations in the absorption intensity of the MS [Fe_3O_4-Ab_2-(PSA)-Ab_1-AuNPs] at 525 nm in the presence of different concentrations of PSA. (C) Interference study of immunosensor. Variations in the absorption intensity of the Ab_1-AuNPs after magnetic separation at 525 nm in present of 10 ng mL^{-1} PSA and 100 ng mL^{-1} Myo, EGFR, VEGF, COR, NSE, HTR, HAS, BSA, AgTR and AgCE and 0.05 mol L^{-1} Na , K , Ca^2 and Mg^2.

this analysis, linear dynamic range (LDR) and limit of detection (LOD) were found to be 0.01–20 ng mL^{-1} and 0.009 ng mL^{-1} with an equation of $\Delta A = 0.1075 \pm 0.0032$ [PSA](ng mL^{-1}) 0.0878 ± 0.0064 (Fig. 3, Panel B). Table 1 represents the main characteristics of the sensing tools and comparison of the immunosensor with this PSA detection methods. This comparison confirms that the sensing tool in this work as a simple and rapid colorimetric method can rival in the sensitivity and limit of detection.

3.3.2. Interference study

For the assessment of immunosensor specificity, assortment of biomarkers including PSA, epidermal growth factor receptor (EGFR), vascular endothelial growth factor (VEGF), cortisol (COR), neuron-specific enolase (NSE), human thrombin (HTR), human albumin serum (HAS), bovine serum albumin (BSA), thrombin antigen (AgTR), myoglobin (Myo),carcinoembryonic antigen (AgCE) and sodium (Na), potassium (K), calcium (Ca^2), magnesium (Mg^2) were investigated for interfering signals. As shown in Fig. 3, Panel C, the maximum change in absorption value was obtained from 10 ng mL^{-1} of PSA, while negligible changes in the absorption intensity were observed in the presence of at least 10-fold higher concentrations of the other tested proteins. The result is indicative of high selectivity of the method, which can be attributed to the high specificity of the antibodies modified nanoparticles toward PSA.

3.3.3. Accuracy, repeatability, stability and reversibility of immunosensor

To demonstrate the viability of the immunosensor in clinical assays, content of PSA in serum samples of healthy donor and prostate cancer patient were analyzed and revalidated by standard ELISA technique. It was observed that there was no significant difference between the results from the immunosensor and ELISA results ($p < 0.05$), confirming the satisfactory accuracy and precision of the immunosensor. In comparison with some parameters, immunosensor represented advantages over ELISA method (Table 2). Moreover, the presence of proteins other than PSA in the serum samples showed no remarkable effect(s) on the sensitivity and specificity of the sensing tool. Since the differences of absorption values was used in the calculations, the effect of background absorption (at 525 nm) in the serum samples was removed in the assays.

For the reversibility of engineered immunosensors, we utilized glycine-HCl (0.15 mol L^{-1}, pH 2.0) in two regeneration cycles for

Table 1
Comparison of the immunosensor with published biosensors for detection of PSA.

Biosensor materials	Technique	LDR (ng mL^{-1})	LOD (pg mL^{-1})	Ref.
Fe_3O_4-TMB-H_2O_2	Photothermometry	1–64	1000	[37]
DNA-AuNPs	Colorimetry		0.182	[38]
PA-Cu-MOG	Fluorescence	0.5–8	330	[39]
GCE-GO@AuNRs-GOD-SA-biotin-DNA	ECL	0.0005–5	0.17	[40]
Ab_1-(PSA)-Ab_2-AuNPS-Cu	Colorimetry		3.4	[41]
PGE-PANI-AuNPs-PNT-Ab_1-Ab_2-HRP	Electrochemistry	1–100	680	[17]
Ab-Au-Bi2Se3 nanosheets	Colorimetry	1–10,000	72	[42]
AuE-DNA-AgNPs-Apt	Electrochemistry	0.001–160	0.11	[43]
AuNPs-ATCUN-Peptide-Fe_3O_4	Colorimetry	0–0.8	20	[44]
Ab_1-(PSA)-Ab_2-HRP-PpyNPs	Colorimetry		0.7	[45]
	Electrochemistry		0.8	
GCE-AuNPs-Ni(OH)$_2$-NGQDs- Ab_1-(PSA)- Ab_2-Fe_3O_4@MnO_2	ECL	0.00001–10	0.000005	[46]
AuE-GRP-PS_{67}-b-PAA_{27}	Electrochemistry	0.0001–100	0.04	[47]
GCE-Au@Pt NCs-Ab	Electrochemistry	0.1–50	18	[48]
Peptide-Fe_3O_4@SiO_2-Au	Fluorescence	0.001–1	0.3	[49]
AuE-MSTF-Apt	Electrochemistry	1–300	280	[50]
Fe_3O_4-Ab_2-(PSA)-Ab_1-AuNPs	Colorimetry	0.01–20	9	This work

Ab: antibody, **AgNPs**: silver nanoparticles, **ATCUN**: amino terminal copper and nickel, **Apt**: aptamer, **Au@Pt NCs**: bimetallic core-shell Au@Pt nanocrystals, **AuE**: gold electrode, **AuNPs**: gold nanoparticles, **AuNRs**: gold nanorods, **Cu-MOG**: Cu-based metal-organic gel, **ECL**: electrochemiluminescence, **GCE**: glassy carbon electrode, **GO**: graphene oxide, **GOD**: glucose oxidase, **GRP**: graphene nanoplatelets, **HRP**: horseradish peroxidase, **NGQDs**: nitrogen-doped graphene quantum dots, **PA**: dye-labeled probe aptamer, **PANI**: polyaniline, **PGE**: pencil graphite electrode, **PNT**: peptide nanotube composite, **PpyNPs**: Polypyrrole nanoparticles, **PS_{67}-b-PAA_{27}**: diblock co-polymer, **SA**: streptavidin, **TMB**: (3,3′,5,5′-tetramethylbenzidine).

Table 2
Real sample analyses and comparison of the immunosensor with a standard ELISA assay.

Patient type	No.	ELISA [PSA] (ng mL^{-1})	Added [PSA] (ng mL^{-1})	Found [PSA] (ng mL^{-1})	Recovery (%)
Healthy individuals	1	1.4 ± 0.3	0	1.37 ± 0.23	97.86 ± 0.77
	1	1.4 ± 0.3	5	6.34 ± 0.41	99.06 ± 1.37
	1	1.4 ± 0.3	10	11.53 ± 0.34	101.14 ± 1.13
Prostate cancer patients	2	6.2 ± 0.2	0	6.33 ± 0.16	102.10 ± 0.80
	2	6.2 ± 0.2	5	11.41 ± 0.32	101.88 ± 1.60
	2	6.2 ± 0.2	10	15.89 ± 0.25	98.09 ± 1.25

3 min. The immunosensor displayed reversibility efficiency of 95.1% ± 1.2 (for five replication) up to 5 cycles with an acceptable reproducibility and precision. In our study, the engineered immunosensors were regenerated in the fixed concentration of PSA (i.e., 10 ng mL^{-1}). Additionally, the engineered Ab_1-AuNPs and Fe_3O_4-Ab_2 were found to be extremely stable at room temperature during 45 and 30 days post-fabrication with coefficient variation percentage (CV%) <5.4% and 5.2% respectively. The reagents of immunoassay were found to be stable up to 90 days at refrigerator temperature (4 °C) and after this period of time, dramatic decrease was observed in the performance of immunosensor.

4. Conclusions

In summary, we have demonstrated the feasibility of a colorimetric immunoassay for determination of PSA using SPR band of colloidal AuNPs. In this work, antibody-conjugated AuNPs were exposed to the PSA antigen molecules in the presence of second antibody-conjugated Fe_3O_4 to form a network of an immune complex. Residual Ab_1-AuNPs (unreacted NPs) were utilized for measurement of SPR signals. This sandwich-type method is simple and rapid, and other signal-producing NPs can be engineered in the platform of this sensing system. However, the sensing approach allows the detection of PSA within the 0.01–20 ng mL^{-1} range of PSA concentrations in real samples. In general, similar to any other sensing platform in which antibody is involved, our assay is faced with the limitation of incubation time (130 min) for completion of antigen-antibody complexation reaction. This incubation time can limit instant analysis of PSA protein. In conclusion, we envisioned that the simple but reliable and efficient platform of this immunosensor to be useful in the development of future point-of-care sensing tools, working on the quantification of biomarkers in a drop of blood.

Author contributions

The manuscript was written through the contributions of all authors. All authors have given approval to the final version of the manuscript.

Acknowledgment

The authors would like to thank National Institute for Medical Research Development (NIMAD) for the financial support this work (Grant No. 957699).

Appendix A. Supplementary data

Supplementary data to this article can be found online at https://doi.org/10.1016/j.saa.2019.117218.

References

[1] M.J. Barry, Prostate-specific–antigen testing for early diagnosis of prostate cancer, N. Engl. J. Med. 344 (2001) 1373–1377, https://doi.org/10.1056/NEJM200105033441806.
[2] F. Bray, J. Ferlay, I. Soerjomataram, R.L. Siegel, L.A. Torre, A. Jemal, Global cancer statistics 2018: GLOBOCAN estimates of incidence and mortality worldwide for 36 cancers in 185 countries, CA Cancer J. Clin. 68 (2018) 394–424, https://doi.org/10.3322/caac.21492.
[3] H.C.B. Graves, M. Kamarei, T.A. Stamey, Identity of prostate specific antigen and the semen protein p30 purified by a rapid chromatography technique, J. Urol. 144 (1990) 1510–1515, https://doi.org/10.1016/S0022-5347(17)39788-4.
[4] J.J. Hlavaty, A.W. Partin, F. Kusinitz, M.J. Shue, A. Stieg, K. Bennett, J.V. Briggman, Mass spectroscopy as a discovery tool for identifying serum markers for prostate cancer, Clin. Chem. 47 (2001) 1924 LP–1926http://clinchem.aaccjnls.org/content/47/10/1924.abstract.
[5] Y. Wang, A. Brunsen, U. Jonas, J. Dostálek, W. Knoll, Prostate specific antigen biosensor based on long range surface plasmon-enhanced fluorescence spectroscopy and dextran hydrogel binding matrix, Anal. Chem. 81 (2009) 9625–9632, https://doi.org/10.1021/ac901662e.
[6] E.E. Kline, E.G. Treat, T.A. Averna, M.S. Davis, A.Y. Smith, L.O. Sillerud, Citrate concentrations in human seminal fluid and expressed prostatic fluid determined via 1H nuclear magnetic resonance spectroscopy outperform prostate specific antigen in prostate cancer detection, J. Urol. 176 (2006) 2274–2279.
[7] G. Koukouvinos, A. Metheniti, C.E. Karachaliou, D. Goustouridis, E. Livaniou, K. Misiakos, I. Raptis, A. Kondili, P. Miniati, P. Petrou, S. Kakabakos, White light reflectance spectroscopy biosensing system for fast quantitative prostate specific antigen determination in forensic samples, Talanta 175 (2017) 443–450, https://doi.org/10.1016/j.talanta.2017.07.074.
[8] M.J. Donohue, M.B. Satterfield, J.J. Dalluge, M.J. Welch, J.E. Girard, D.M. Bunk, Capillary electrophoresis for the investigation of prostate-specific antigen heterogeneity, Anal. Biochem. 339 (2005) 318–327, https://doi.org/10.1016/j.ab.2005.01.043.
[9] Y. Zheng, H. Chen, X.-P. Liu, J.-H. Jiang, Y. Luo, G.-L. Shen, R.-Q. Yu, An ultrasensitive chemiluminescence immunosensor for PSA based on the enzyme encapsulated liposome, Talanta 77 (2008) 809–814.
[10] L.I. Stowell, L.E. Sharman, K. Hamel, An enzyme-linked immunosorbent assay (ELISA) for prostate-specific antigen, Forensic Sci. Int. 50 (1991) 125–138, https://doi.org/10.1016/0379-0738(91)90141-5.
[11] F. Zhang, L. Mao, M. Zhu, Ultrasensitive immunoassay for free prostate-specific antigen based on ferrocenecarboxylate enhanced cathodic electrochemiluminescence of peroxydisulfate, Microchim. Acta 181 (2014) 1285–1291, https://doi.org/10.1007/s00604-014-1240-7.
[12] S.M. Khoshfetrat, H. Khoshsafar, A. Afkhami, M.A. Mehrgardi, H. Bagheri, Enhanced visual wireless electrochemiluminescence immunosensing of prostate-specific antigen based on the luminol loaded into MIL-53 (Fe)-NH2 accelerator and hydrogen evolution reaction mediation, Anal. Chem. 91 (2019) 6383–6390.
[13] G. Sun, H. Liu, Y. Zhang, J. Yu, M. Yan, X. Song, W. He, Gold nanorods-paper electrode based enzyme-free electrochemical immunoassay for prostate specific antigen using porous zinc oxide spheres-silver nanoparticles nanocomposites as labels, New J. Chem. 39 (2015) 6062–6067, https://doi.org/10.1039/c5nj00629e.
[14] T. Soukka, J. Paukkunen, H. Härmä, S. Lönnberg, H. Lindroos, T. Lövgren, Supersensitive time-resolved immunofluorometric assay of free prostate-specific antigen with nanoparticle label technology, Clin. Chem. 47 (2001) 1269–1278.
[15] T. Kaya, T. Kaneko, S. Kojima, Y. Nakamura, Y. Ide, K. Ishida, Y. Suda, K. Yamashita, High-sensitivity immunoassay with surface plasmon field-enhanced fluorescence spectroscopy using a plastic sensor chip: application to quantitative analysis of total prostate-specific antigen and GalNAcβ1-4GlcNAc-linked prostate-specific antigen for prost, Anal. Chem. 87 (2015) 1797–1803, https://doi.org/10.1021/ac503735e.
[16] Y. Seto, T. Iba, K. Abe, Development of ultra-high sensitivity bioluminescent enzyme immunoassay for prostate-specific antigen (PSA) using firefly luciferase, Luminescence 16 (2001) 285–290, https://doi.org/10.1002/bio.654.
[17] T. Vural, Y.T. Yaman, S. Ozturk, S. Abaci, E.B. Denkbas, Electrochemical immunoassay for detection of prostate specific antigen based on peptide nanotube-gold nanoparticle-polyaniline immobilized pencil graphite electrode, J. Colloid Interface Sci. 510 (2018) 318–326, https://doi.org/10.1016/j.jcis.2017.09.079.
[18] N. Chen, M. Rong, X. Shao, H. Zhang, S. Liu, B. Dong, W. Xue, T. Wang, T. Li, J. Pan, Surface-enhanced Raman spectroscopy of serum accurately detects prostate cancer in patients with prostate-specific antigen levels of 4–10 ng/mL, Int. J. Nanomedicine Volume 12 (2017) 5399–5407, https://doi.org/10.2147/IJN.S137756.
[19] J.H. Lee, K.S. Hwang, J. Park, K.H. Yoon, D.S. Yoon, T.S. Kim, Immunoassay of prostate-specific antigen (PSA) using resonant frequency shift of piezoelectric nanomechanical microcantilever, Biosens. Bioelectron. 20 (2005) 2157–2162, https://doi.org/10.1016/j.bios.2004.09.024.
[20] V.K. Gupta, A.K. Singh, L.K. Kumawat, Thiazole Schiff base turn-on fluorescent chemosensor for Al3 ion, Sensors Actuators B Chem. 195 (2014) 98–108, https://doi.org/10.1016/j.snb.2013.12.092.
[21] V.K. Gupta, N. Mergu, L.K. Kumawat, A.K. Singh, Selective naked-eye detection of Magnesium (II) ions using a coumarin-derived fluorescent probe, Sensors Actuators B Chem. 207 (2015) 216–223, https://doi.org/10.1016/j.snb.2014.10.044.

[22] V.K. Gupta, N. Mergu, L.K. Kumawat, A.K. Singh, A reversible fluorescence "off–on–off" sensor for sequential detection of aluminum and acetate/fluoride ions, Talanta 144 (2015) 80–89, https://doi.org/10.1016/j.talanta.2015.05.053.
[23] M.L. Yola, V.K. Gupta, T. Eren, A.E. Şen, N. Atar, A novel electro analytical nanosensor based on graphene oxide/silver nanoparticles for simultaneous determination of quercetin and morin, Electrochim. Acta 120 (2014) 204–211, https://doi.org/10.1016/j.electacta.2013.12.086.
[24] K.E. Sapsford, W.R. Algar, L. Berti, K.B. Gemmill, B.J. Casey, E. Oh, M.H. Stewart, I.L. Medintz, Functionalizing nanoparticles with biological molecules: developing chemistries that facilitate nanotechnology, Chem. Rev. 113 (2013) 1904–2074, https://doi.org/10.1021/cr300143v.
[25] H. Karimi-Maleh, F. Tahernejad-Javazmi, N. Atar, M.L. Yola, V.K. Gupta, A.A. Ensafi, A novel DNA biosensor based on a pencil graphite electrode modified with polypyrrole/functionalized multiwalled carbon nanotubes for determination of 6-mercaptopurine anticancer drug, Ind. Eng. Chem. Res. 54 (2015) 3634–3639, https://doi.org/10.1021/ie504438z.
[26] V. Gupta, H. Karimi-maleh, R. Sadeghi, Simultaneous determination of hydroxylamine, phenol and sulfite in water and waste water samples using a voltammetric nanosensor, Int. J. Electrochem. Sci. 10 (2014) 303–316.
[27] A. Asfaram, M. Ghaedi, S. Agarwal, I. Tyagi, V.K. Gupta, Removal of basic dye Auramine-O by ZnS:Cu nanoparticles loaded on activated carbon: optimization of parameters using response surface methodology with central composite design, RSC Adv. 5 (2015) 18438–18450, https://doi.org/10.1039/c4ra15637d.
[28] V.K. Gupta, N. Atar, M.L. Yola, Z. Üstündağ, L. Uzun, A novel magnetic Fe@ Au core–shell nanoparticles anchored graphene oxide recyclable nanocatalyst for the reduction of nitrophenol compounds, Water Res. 48 (2014) 210–217.
[29] L.H. Reddy, J.L. Arias, J. Nicolas, P. Couvreur, Magnetic nanoparticles: design and characterization, toxicity and biocompatibility, pharmaceutical and biomedical applications, Chem. Rev. 112 (2012) 5818–5878, https://doi.org/10.1021/cr300068p.
[30] J. Sun, Y. Xianyu, X. Jiang, Point-of-care biochemical assays using gold nanoparticle-implemented microfluidics, Chem. Soc. Rev. 43 (2014) 6239–6253, https://doi.org/10.1039/C4CS00125G.
[31] M.R. Hormozi-Nezhad, P. Karami, H. Robatjazi, A simple shape-controlled synthesis of gold nanoparticles using nonionic surfactants, RSC Adv. 3 (2013) 7726–7732.
[32] P. Hashemi, H. Bagheri, A. Afkhami, Y. Hosseinzadeh Ardakani, T. Madrakian, Fabrication of a Novel Aptasensor Based on Three-Dimensional Reduced Graphene Oxide/Polyaniline/Gold Nanoparticle Composite as a Novel Platform for High Sensitive and Specific Cocaine Detection, 996, 2017 10–19.
[33] J.M. Perez, Iron oxide nanoparticles: hidden talent, Nat. Nanotechnol. 2 (2007) 535.
[34] R. De Palma, S. Peeters, M.J. Van Bael, H. den Rul, K. Bonroy, W. Laureyn, J. Mullens, G. Borghs, G. Maes, Silane ligand exchange to make hydrophobic superparamagnetic nanoparticles water-dispersible, Chem. Mater. 19 (2007) 1821–1831, https://doi.org/10.1021/cm0628000.
[35] T. Sannomiya, C. Hafner, J. Vörös, Shape-dependent sensitivity of single plasmonic nanoparticles for biosensing, J. Biomed. Opt. 14 (2009) 064027, https://doi.org/10.1117/1.3269678.
[36] S. Ahmed, S. Ikram, Synthesis of gold nanoparticles using plant extract: an overview, iMedPub, n.d. http://nanotechnology.imedpub.com/synthesis-of-gold-nanoparticles-using-plant-extract-an-overview.php?aid=7649 (accessed May 10, 2019).
[37] G. Fu, S.T. Sanjay, W. Zhou, R.A. Brekken, R.A. Kirken, X. Li, Exploration of nanoparticle-mediated photothermal effect of TMB-H2O2 colorimetric system and its application in a visual quantitative photothermal immunoassay, Anal. Chem. 90 (2018) 5930–5937, https://doi.org/10.1021/acs.analchem.8b00842.
[38] X. Kou, T. Liu, X. Yang, Y. Tang, X. Gong, P. Miao, Role of Tripodal DNA modified gold nanoparticles in colorimetric aptasensing, Colloid Interface Sci. Commun. 21 (2017) 19–21, https://doi.org/10.1016/j.colcom.2017.11.001.
[39] T.T. Zhao, Z.W. Peng, D. Yuan, S.J. Zhen, C.Z. Huang, Y.F. Li, Metal-organic gel enhanced fluorescence anisotropy for sensitive detection of prostate specific antigen, Spectrochim. Acta A Mol. Biomol. Spectrosc. 192 (2018) 328–332, https://doi.org/10.1016/j.saa.2017.10.072.
[40] J.-T. Cao, J.-J. Yang, L.-Z. Zhao, Y.-L. Wang, H. Wang, Y.-M. Liu, S.-H. Ma, Graphene oxide@ gold nanorods-based multiple-assisted electrochemiluminescence signal amplification strategy for sensitive detection of prostate specific antigen, Biosens. Bioelectron. 99 (2018) 92–98.
[41] Y. Liu, Z. Zhang, J. Yu, J. Xie, C.M. Li, A concentration–dependent multicolor conversion strategy for ultrasensitive colorimetric immunoassay with the naked eye, Anal. Chim. Acta 963 (2017) 129–135, https://doi.org/10.1016/j.aca.2017.01.034.
[42] L. Xiao, A. Zhu, Q. Xu, Y. Chen, J. Xu, J. Weng, Colorimetric biosensor for detection of cancer biomarker by au nanoparticle-decorated Bi2Se3 nanosheets, ACS Appl. Mater. Interfaces 9 (2017) 6931–6940, https://doi.org/10.1021/acsami.6b15750.
[43] P. Miao, Y. Jiang, Y. Wang, J. Yin, Y. Tang, An electrochemical approach capable of prostate specific antigen assay in human serum based on exonuclease-aided target recycling amplification, Sensors Actuators B Chem. 257 (2018) 1021–1026, https://doi.org/10.1016/j.snb.2017.11.064.
[44] N. Xia, D. Deng, Y. Wang, C. Fang, S.-J. Li, Gold nanoparticle-based colorimetric method for the detection of prostate-specific antigen, Int. J. Nanomedicine 13 (2018) 2521–2530, https://doi.org/10.2147/IJN.S154046.
[45] W. Hong, S. Lee, Y. Cho, Dual-responsive immunosensor that combines colorimetric recognition and electrochemical response for ultrasensitive detection of cancer biomarkers, Biosens. Bioelectron. 86 (2016) 920–926, https://doi.org/10.1016/j.bios.2016.07.014.
[46] W. Zhu, M.S. Khan, W. Cao, X. Sun, H. Ma, Y. Zhang, Q. Wei, Ni(OH)2/NGQDs-based electrochemiluminescence immunosensor for prostate specific antigen detection by coupling resonance energy transfer with Fe3O4@MnO2 composites, Biosens. Bioelectron. 99 (2018) 346–352, https://doi.org/10.1016/j.bios.2017.08.005.
[47] M.S. Khan, K. Dighe, Z. Wang, I. Srivastava, E. Daza, A.S. Schwartz-Dual, J. Ghannam, S.K. Misra, D. Pan, Detection of prostate specific antigen (PSA) in human saliva using an ultra-sensitive nanocomposite of graphene nanoplatelets with diblock-: Co-polymers and Au electrodes, Analyst 143 (2018) 1094–1103, https://doi.org/10.1039/c7an01932g.
[48] R. Wang, A.J. Wang, W.D. Liu, P.X. Yuan, Y. Xue, X. Luo, J.J. Feng, A novel label-free electrochemical immunosensor for ultra-sensitively detecting prostate specific antigen based on the enhanced catalytic currents of oxygen reduction catalyzed by core-shell Au@Pt nanocrystals, Biosens. Bioelectron. 102 (2018) 276–281, https://doi.org/10.1016/j.bios.2017.11.041.
[49] L. Yang, N. Li, K. Wang, X. Hai, J. Liu, F. Dang, A novel peptide/Fe3O4@SiO2-Au nanocomposite-based fluorescence biosensor for the highly selective and sensitive detection of prostate-specific antigen, Talanta 179 (2018) 531–537, https://doi.org/10.1016/j.talanta.2017.11.033.
[50] W. Argoubi, A. Sánchez, C. Parrado, N. Raouafi, R. Villalonga, Label-free electrochemical aptasensing platform based on mesoporous silica thin film for the detection of prostate specific antigen, Sensors Actuators B Chem. 255 (2018) 309–315, https://doi.org/10.1016/j.snb.2017.08.045.